PHYSICAL REVIEW D **96,** 115009 (2017)

Off-diagonal dark-matter phenomenology: Exploring enhanced complementarity relations in nonminimal dark sectors

Keith R. Dienes,[1,2,*] Jason Kumar,[3,†] Brooks Thomas,[4,‡] and David Yaylali[1,§]

[1]*Department of Physics, University of Arizona, Tucson, Arizona 85721, USA*
[2]*Department of Physics, University of Maryland, College Park, Maryland 20742, USA*
[3]*Department of Physics and Astronomy, University of Hawaii, Honolulu, Hawaii 96822, USA*
[4]*Department of Physics, Lafayette College, Easton, Pennsylvania 18042, USA*

(Received 11 September 2017; published 15 December 2017)

In most multicomponent dark-matter scenarios, two classes of processes generically contribute to event rates at experiments capable of probing the nature of the dark sector. The first class consists of "diagonal" processes involving only a single species of dark-matter particle—processes analogous to those which arise in single-component dark-matter scenarios. By contrast, the second class consists of "off-diagonal" processes involving dark-matter particles of different species. Such processes include inelastic scattering at direct-detection experiments, asymmetric production at colliders, dark-matter co-annihilation, and certain kinds of dark-matter decay. In typical multicomponent scenarios, the contributions from diagonal processes dominate over those from off-diagonal processes. Unfortunately, this tends to mask those features which are most sensitive to the multicomponent nature of the dark sector. In this paper, by contrast, we point out that there exist natural, multicomponent dark-sector scenarios in which the off-diagonal contributions actually dominate over the diagonal. This then gives rise to a new, enhanced picture of dark-matter complementarity. In this paper, we introduce a scenario in which this situation arises and examine the enhanced picture of dark-matter complementarity which emerges.

DOI: 10.1103/PhysRevD.96.115009

I. INTRODUCTION

Overwhelming evidence suggests that particle dark matter contributes a substantial fraction of the present-day energy density in the Universe [1]. All of this evidence ultimately relies upon gravitational interactions between the dark matter and visible matter. However, it is possible that the fields constituting the dark matter may interact with the fields of the Standard Model (SM) in other ways as well. This possibility has inspired a number of experimental strategies for observing dark matter, including direct detection, indirect detection, and collider searches.

In typical theoretical dark-matter models, the underlying amplitudes which provide the leading contributions to dark-matter production, scattering, and annihilation rates are related by crossing symmetries. For this reason, different experimental probes of the dark sector can be seen as complementary in two ways. First, these different probes explore different regions of the parameter space of a given dark-matter model. Second, the comparison of results from multiple such probes can assist us in distinguishing between different models. In this way, the complementarities between different experimental probes of the dark sector can provide a useful tool for exploring and constraining the parameter space of a particular dark-matter model (for a review, see, e.g., Ref. [2]).

In multicomponent dark-matter scenarios, however, the experimental complementarity picture can be even richer and more subtle than it is in traditional, single-component scenarios [3]. One reason is that the multicomponent nature of the dark sector allows for two distinct classes of processes which can generically contribute to the relevant experimental event rates. The first class consists of "diagonal" processes involving only a single species of dark-matter particle. These processes, which are analogous to those which arise in single-component dark-matter scenarios, include the elastic scattering of dark matter with visible matter, dark-matter annihilation, and symmetric pair-production processes at colliders. By contrast, the second class consists of "off-diagonal" processes involving two dark-matter particles of different species. These processes include the inelastic scattering of dark matter with visible matter, dark-matter co-annihilation, and asymmetric pair-production processes at colliders. Moreover, this latter class also includes a wholly different type of process that has no analogue in single-component dark-matter models: the decay of a heavier dark-matter species to a final state comprising a lighter dark-matter species and some number of SM particles [3]. Since the underlying amplitudes associated with dark-matter decay processes are also generally related through crossing symmetries to the amplitudes associated with dark-matter production, scattering, and annihilation, the web of dark-matter complementarity

*dienes@email.arizona.edu
†jkumar@hawaii.edu
‡thomasbd@lafayette.edu
§yaylali@email.arizona.edu

relations in multicomponent dark-matter scenarios is significantly enhanced relative to that which emerges in single-component scenarios.

In multicomponent dark-matter scenarios, both diagonal and off-diagonal processes in principle contribute to the signal-event rates at direct- and indirect-detection experiments and at colliders. Indeed, both diagonal and off-diagonal processes are usually permitted by the symmetries of the theory. However, it turns out that the off-diagonal processes generically play only a subleading role in the phenomenology of such scenarios. There are a variety of reasons for this. At direct-detection experiments, for example, the rates for up-scattering processes (i.e., inelastic processes in which a lighter dark-matter particle scatters into a heavier dark-matter particle) are suppressed due to the scattering kinematics. On the other hand, down-scattering processes (i.e., so-called "exothermic" processes in which a heavier dark-matter particle scatters into a lighter dark-matter particle) frequently yield a nuclear recoil energy sufficiently large that the corresponding events are vetoed by cuts imposed to reduce experimental backgrounds. Likewise, at indirect-detection experiments, the contribution to the event rate from a co-annihilation process is proportional to the energy density of each of the two dark-matter species involved. Thus, in cases in which the primordial abundance of one of the two species is significantly depleted by decays prior to the present epoch, this co-annihilation contribution is generically suppressed. Finally, in many multicomponent dark-matter scenarios, the mixing among different dark-matter species is the result of the controlled breaking of approximate symmetries. In such scenarios, the Lagrangian couplings associated with off-diagonal processes are often suppressed relative to those associated with the corresponding diagonal processes, independent of any kinematic or cosmological considerations.

In such models, then, it is the diagonal processes which tend to provide the dominant contribution to the observed event rates at relevant experiments. This is unfortunate, since this dominance of the diagonal processes tends to mask precisely those features which are most sensitive to the multicomponent nature of the dark sector.

For this reason, discovery and exploration of a potential multicomponent dark sector would be greatly facilitated if such a sector somehow incorporated a method of forbidding or suppressing the contributions from diagonal processes. This would allow off-diagonal processes to shine through and have a significant impact on the resulting phenomenology. Fortunately, as we shall see in this paper, there exist many multicomponent dark-matter scenarios in which this is precisely what occurs—scenarios in which the diagonal processes that would otherwise provide the dominant contributions to relevant experimental event rates are forbidden or suppressed. In such scenarios, the corresponding off-diagonal processes then effectively dictate the phenomenology of the dark sector, and even give rise to a distinct, enhanced picture of dark-matter complementarity.

This paper is organized as follows. In Sec. II, we discuss the circumstances under which off-diagonal processes provide the dominant contribution to event rates at direct-detection experiments, at indirect-detection experiments, and at colliders. We also present a concrete example of a scenario in which this situation naturally arises. In Sec. III, we then discuss the phenomenological implications of this dominance of off-diagonal processes and evaluate the cross sections and decay widths for the relevant physical processes. In Sec. IV, we then focus on the experimental and observational considerations which constrain the parameter space of our off-diagonal dark-matter scenario, and in Sec. V we examine the combined constraints on this parameter space and assess the extent to which future dark-matter experiments will be able to probe its currently unconstrained regions. Finally, in Sec. VI, we discuss the implications of our results and possible directions for future work.

II. OFF-DIAGONAL INTERACTIONS

As discussed in the Introduction, we are interested in exploring the phenomenology of dark-matter scenarios in which off-diagonal processes provide the dominant contribution to event rates at dark-matter detection experiments. We shall now provide an explicit model in which this is precisely what occurs.

For concreteness, we shall focus on the case in which the dark-matter particles χ_i are spin-$1/2$ fermions. We shall also focus on the regime in which the leading interactions between the dark and visible sectors at low energies can be modeled by a set of contact operators which are separately invariant under charge-conjugation C, parity P, and time-reversal T. For simplicity, we shall focus on the case in which the χ_i couple to the SM fields primarily via dimension-six operators of the form

$$\mathcal{O}^{(\alpha)}_{ijq} = \frac{c^{(\alpha)}_{ijq}}{\Lambda^2}[\bar{\chi}_i\Gamma^{(\alpha)}\chi_j][\bar{q}\Gamma^{(\alpha)}q], \tag{2.1}$$

where q denotes a SM quark, where Λ denotes the scale of new physics, and where $c^{(\alpha)}_{ijq}$ are dimensionless coupling coefficients. The label α indicates the gamma-matrix structure of the fermion bilinears, with $\alpha = \{S, P, V, A, T\}$ corresponding to $\Gamma^{(\alpha)} = \{1, \gamma^5, \gamma^\mu, \gamma^\mu\gamma^5, \sigma^{\mu\nu}\}$, respectively. Operators with $i = j$ give rise to "diagonal" processes involving two of the same dark-sector particle, while operators with $i \neq j$ give rise to "off-diagonal" processes involving two different dark-sector particles.

As discussed in the Introduction, when operators with $i = j$ and operators with $i \neq j$ are both present with similar values of $c^{(\alpha)}_{ijq}$, the operators with $i = j$ tend to play a dominant role in dark-matter phenomenology. In this paper,

by contrast, we are primarily interested in studying the alternative possibility in which off-diagonal processes are dominant. There are several ways in which this naturally can occur. One observation which we shall exploit in this paper is that if χ_i are Majorana rather than Dirac fermions, the vector and antisymmetric tensor operators $\mathcal{O}^{(V)}_{ijq}$ and $\mathcal{O}^{(T)}_{ijq}$ both vanish identically when $i = j$. Thus, in cases in which the primary coupling between such Majorana χ_i and the visible sector occurs through such operators, off-diagonal processes indeed play the dominant role in the resulting phenomenology.

In order to develop this model more fully, let us assume that the dark sector includes a vectorlike Dirac fermion χ, which comprises a left-handed Weyl spinor $\chi_{L\alpha}$ and a right-handed conjugate Weyl spinor $\chi_R^{\dagger\dot{\alpha}}$, as well as a complex scalar ζ. We shall assume that the action for these dark-sector fields is invariant under an additional $U(1)'$ gauge symmetry, as well as the discrete symmetries C, P, and T. Moreover, we shall assume that the $U(1)'$ charges Q'_χ and Q'_ζ for these fields are chosen such that $Q'_\zeta = -2Q'_\chi$. Such a charge assignment permits a Yukawa-type interaction of the form

$$\mathcal{L}_{\rm Yuk} = -y\zeta\bar{\chi}\chi^c + \text{H.c.}, \tag{2.2}$$

where y is a real, dimensionless Yukawa coupling and where $\chi^c \equiv C^{-1}\bar{\chi}C$ is the charge-conjugate of χ. Note that all of the operators given in Eq. (2.1) with $\chi_i = \chi_j = \chi$ are consistent with the symmetries of the theory as well.

If the scalar ζ acquires a vacuum expectation value (VEV) as a result of some additional dynamics, this VEV breaks $U(1)'$ and generates a Majorana mass $m_M = 2y\langle\zeta\rangle$ for χ while leaving C, P, and T intact. Moreover, since χ is vectorlike, a Dirac mass m_D for χ is also consistent with all symmetries of the theory and is therefore generically expected to be present as well. Thus, once ζ acquires a VEV, the mass matrix for the Weyl spinors $\chi_{L\alpha}$ and $\chi_{R\alpha}$ generically takes the form

$$\mathcal{L}_{\rm mass} = -\frac{1}{2}(\chi_L^\alpha, \chi_R^\alpha)\begin{pmatrix} m_M & m_D \\ m_D & m_M \end{pmatrix}\begin{pmatrix} \chi_{L\alpha} \\ \chi_{R\alpha} \end{pmatrix} + \text{H.c.} \tag{2.3}$$

The mass eigenstates of the theory, obtained by diagonalizing this matrix, can therefore be viewed as a pair of Majorana fermions [4]

$$\chi_1 = \frac{i}{\sqrt{2}}\begin{pmatrix} \chi_{L\alpha} - \chi_{R\alpha} \\ \chi_L^{\dagger\dot{\alpha}} - \chi_R^{\dagger\dot{\alpha}} \end{pmatrix},$$
$$\chi_2 = \frac{1}{\sqrt{2}}\begin{pmatrix} \chi_{L\alpha} + \chi_{R\alpha} \\ \chi_L^{\dagger\dot{\alpha}} + \chi_R^{\dagger\dot{\alpha}} \end{pmatrix}, \tag{2.4}$$

with respective masses $m_1 = m_D - m_M$ and $m_2 = m_D + m_M$. Moreover, since m_M is generated dynamically, the mass splitting $\Delta m \equiv m_2 - m_1 = 2m_M$ between these two mass eigenstates can naturally be small.

Let us assume, for the moment, that amongst the operators in Eq. (2.1), the vector and antisymmetric-tensor operators dominate. In such a case, the full interaction Lagrangian $\mathcal{L}_{\rm int}$ between the dark and visible sectors receives contributions from the two operators

$$\mathcal{L}^{(V)}_{\rm int} = \sum_q \frac{2c_q^{(V)}}{\Lambda^2}(\bar{\chi}\gamma^\mu\chi)(\bar{q}\gamma_\mu q),$$
$$\mathcal{L}^{(T)}_{\rm int} = \sum_q \frac{2c_q^{(T)}}{\Lambda^2}(\bar{\chi}\sigma^{\mu\nu}\chi)(\bar{q}\sigma_{\mu\nu} q). \tag{2.5}$$

However, when these operators are expressed in terms of the mass eigenstates in Eq. (2.4), the diagonal terms vanish [4,5]. The resulting interactions between the dark and visible sectors are therefore purely off-diagonal, as desired:

$$\mathcal{L}^{(V)}_{\rm int} = \sum_q \left[\frac{ic_q^{(V)}}{\Lambda^2}(\bar{\chi}_1\gamma^\mu\chi_2 - \bar{\chi}_2\gamma^\mu\chi_1)(\bar{q}\gamma_\mu q)\right],$$
$$\mathcal{L}^{(T)}_{\rm int} = \sum_q \left[\frac{ic_q^{(T)}}{\Lambda^2}(\bar{\chi}_1\sigma^{\mu\nu}\chi_2 - \bar{\chi}_2\sigma^{\mu\nu}\chi_1)(\bar{q}\sigma_{\mu\nu} q)\right]. \tag{2.6}$$

Indeed, these are the two interaction terms whose phenomenological effects we shall study in the rest of this paper.

Of course, the success of this scenario is predicated on the assumption that only the vector and tensor interactions dominate from amongst all the operators in Eq. (2.1). If we had assumed non-negligible coefficients for any of the other operators in Eq. (2.1) and expressed such operators in terms of our mass eigenstates, both diagonal and off-diagonal operator interactions would have appeared. However, the operators in Eq. (2.1) are only effective operators valid for energies below Λ. Thus the question of which operators actually appear in our effective low-energy theory below Λ depends critically on the physics we assume to exist at higher energy scales above Λ.

It is not hard to demonstrate that there exist scenarios in which only the vector and/or tensor operators can be generated in the effective theory below Λ. For example, let us imagine that the interaction between the dark-sector fermions and the SM quarks arises due to integrating out the massive gauge boson Z'^μ associated with the $U(1)'$ symmetry discussed above. In particular, let us take the Lagrangian for the dark-sector fields χ, ζ, and Z'^μ to be

$$\mathcal{L} = i\bar{\chi}\not{D}\chi + D^\mu\zeta^\dagger D_\mu\zeta - V(\zeta,\zeta^\dagger) - m_D\bar{\chi}\chi$$
$$- y\zeta\bar{\chi}\chi^c - y\zeta^\dagger\overline{\chi^c}\chi - \frac{1}{4}F'_{\mu\nu}F'^{\mu\nu}. \tag{2.7}$$

Here $F'^{\mu\nu} \equiv (\partial^\mu Z'^\nu - \partial^\nu Z'^\mu)$ is the field-strength tensor for Z'^μ, while y is a real Yukawa coupling, $V(\zeta,\zeta^\dagger)$ is the scalar

potential for ζ and its Hermitian conjugate $\zeta^\dagger$, and the covariant derivatives D_μ are given by $D_\mu\chi \equiv \partial_\mu\chi - ig'Q_\chi Z\chi$ and $D_\mu\zeta \equiv \partial_\mu\zeta - ig'Q_\zeta Z\zeta$, where g' is the gauge coupling constant for the $U(1)'$ interaction. As discussed above, we assume that $V(\zeta,\zeta^\dagger)$ is such that ζ acquires a VEV $\langle\zeta\rangle$ which in turn spontaneously breaks $U(1)'$ and gives a mass $M_{Z'}$ to Z'^μ. If the SM quarks are also charged under $U(1)'$, we may integrate out Z'^μ at scales well below $M_{Z'}$ in order to obtain a set of effective operators coupling χ to the SM quarks. In particular, the resulting effective Lagrangian contains the terms

$$\mathcal{L}_{\rm eff} \ni \sum_q \frac{g'^2 Q_q Q_\chi}{M_{Z'}^2}(\bar\chi\gamma^\mu\chi)(\bar q\gamma_\mu q), \tag{2.8}$$

where Q_q is the $U(1)'$ charge of quark q. Moreover, when ζ acquires a VEV, a Majorana mass $m_M = 2y\langle\zeta\rangle$ is generated for the dark-sector fermions, as discussed above.

Most importantly, however, we see that upon converting to the mass eigenbasis the resulting operators in Eq. (2.7) take the vector-operator form appearing in Eq. (2.6). Indeed, we can now identify Λ in terms of the parameters of our underlying theory via $c_q^{(V)}/\Lambda^2 \sim g'^2 Q_q Q_\chi/M_{Z'}^2$. Moreover, no other operator with a different Lorentz structure appears below Λ at leading order.

Of course, it is always possible to add additional interaction terms in our ultraviolet (UV) theory in Eq. (2.7) in order to generate the full spectrum of effective operators in Eq. (2.1) at low energies. Thus the question of what is fully "natural" becomes a question of presupposing a particular UV theory—a task which is beyond the scope of this paper. We have nevertheless demonstrated that the model presented in this section gives rise to off-diagonal interactions while at the same time suppressing diagonal interactions—all emerging in a unified way from the assumption of a simple Lorentz structure for our dimension-six effective interactions between the dark and visible sectors.

III. RATES AND CROSS SECTIONS

Off-diagonal dark-matter scenarios exhibit a rich set of complementarity relations [3]. Indeed, as discussed in the Introduction and in Ref. [3], a single off-diagonal operator can simultaneously give rise to inelastic up-scattering and down-scattering processes at direct-detection experiments, dark-matter co-annihilation processes relevant for indirect detection, asymmetric dark-matter production at colliders, and decay processes in which a heavier dark-matter particle decays into a lighter one. In this section, we evaluate the cross sections and decay rates for these processes.

We shall perform these calculations within the framework of the model introduced in Sec. II. Specifically, we shall imagine that the dark sector comprises two Majorana fermions χ_1 and χ_2 with masses m_1 and m_2 which couple to the SM quarks through either of the operators in Eq. (2.6). Without loss of generality we shall take $m_2 > m_1$ so that the mass splitting $\Delta m \equiv m_2 - m_1$ is positive-definite. In what follows, we shall also focus on the regime in which $\Delta m \lesssim \mathcal{O}(\text{MeV}) \ll m_1 \approx m_2$, as this is the regime in which inelastic processes have a demonstrable impact on direct-detection phenomenology and in which χ_2 can be sufficiently long-lived as to have observable consequences for indirect detection. In other words, this is the regime in which the off-diagonal nature of the dark-sector interactions truly matters. Finally, we shall assume that the dark-sector fields only couple to first-generation quarks—i.e., we shall take $c_q^{(V)} = c_q^{(T)} = 0$ for $q \in \{c,s,b,t\}$ within the operators in Eq. (2.6). We shall then calculate our cross sections and decay rates for these two operators respectively.

Of course, the direct- and indirect-detection phenomenology of our scenario depends not only on the particle-physics properties of our dark-sector fields, but also on their astrophysical properties—and in particular, on their cosmological abundances. We shall therefore assume that the contributions from χ_1 and χ_2 together constitute essentially the entire dark-matter abundance $\Omega_{\rm DM} \approx 0.26$ [6] at present time $t_{\rm now}$. We likewise assume that initial number densities $n_1(t_0)$ and $n_2(t_0)$ are established at some early time $t_0 \ll t_{\rm now}$, and that the only subsequent change in these number densities, other than the usual dilution resulting from Hubble expansion, is due to dark-matter co-annihilation or decay processes following from one of the operators in Eq. (2.6). Since the co-annihilation rate at time t is proportional to the product $n_1(t)n_2(t)$ while the depletion rate of χ_2 due to decays is proportional to $n_2(t)$ alone, it is sufficient to focus on decays. For the operators in Eq. (2.6), each decay of a χ_2 particle produces a χ_1 particle and thus the total comoving number density $n_{\rm tot}(t) = n_1(t) + n_2(t)$ of dark-matter particles is "conserved" in the sense that its only time dependence comes from Hubble expansion rather than net particle creation/annihilation. Therefore, if we define the initial fractions $f_i(t) \equiv n_i(t)/n_{\rm tot}(t)$ of the dark-matter number density contributed by χ_i at any time t, we have at present time

$$\begin{aligned} f_2(t_{\rm now}) &= f_2(t_0)e^{-(t_{\rm now}-t_0)/\tau_2}, \\ f_1(t_{\rm now}) &= 1 - f_2(t_{\rm now}), \end{aligned} \tag{3.1}$$

where τ_2 is the lifetime of χ_2. In particular, all effects due to Hubble expansion are eliminated from the f_i. Moreover, since we have assumed that $\Delta m \ll m_1 \approx m_2$, we see that $f_1(t_{\rm now})$ and $f_2(t_{\rm now})$ are to a very good approximation equal to the fractions of $\Omega_{\rm DM}$ contributed by the respective dark-matter particles.

In what follows, we shall take the *primordial* number-density fraction $f_2(t_0)$ to be the free parameter which characterizes the relative abundances or number densities of the dark-matter particles. Moreover, in order to distinguish

between the vector or tensor cases [i.e., in order to distinguish between the two interaction Lagrangians in Eq. (2.6)], we shall adopt the notation $f_{1,2}^{(V,A)} \equiv f_{1,2}(t_0)$ for these two cases, respectively.

A. Decay rates

As stressed in Ref. [3], one of the most important and unique consequences of off-diagonal interactions among the dark-sector fields is the possibility for a heavier dark-matter particle to decay into a lighter dark-matter particle plus additional SM fields. In the regime in which $\Delta m \lesssim 1$ MeV, the only SM particles which can appear in the final state are photons and neutrinos. Since decay processes involving neutrinos are generically suppressed relative to those involving photons alone, we focus exclusively on the latter.

The operators in Eq. (2.6) which describe the microscopic interactions between our dark-sector particles χ_i and SM quarks ultimately give rise to effective interactions between χ_1, χ_2, and the photon field in the low-energy, macroscopic theory. The structure of the corresponding effective operators can be computed, for example, within the framework of chiral perturbation theory. However, the structure of the leading operators can also be inferred simply from symmetry considerations. For example, we note that both the vector-current density $\chi_i\gamma^\mu\chi_j$ and the tensor-current density $\chi_i\sigma^{\mu\nu}\chi_j$ are odd under charge conjugation. Since the photon field is likewise C-odd, each of these operators can only couple to an odd number of photons. Thus, naïvely, one would expect that the leading contribution to the decay width of χ_2 would arise due to the two-body process $\chi_2 \to \chi_1\gamma$.

However, for dark-sector particles which couple to the visible sector primarily through the vector operator in Eq. (2.6), there is an additional consideration which one must take into account. Specifically, the Ward identity prohibits the coupling of a current operator of the form $\bar{\chi}_i\gamma^\mu\chi_j$ with $i \neq j$ to a single photon. The leading contribution to the decay width of χ_2 is therefore associated with the four-body decay process $\chi_2 \to \chi_1\gamma\gamma\gamma$. Contributions to this process can arise both from contact interactions involving the dark-sector fields and the photon field alone and from processes involving a photon and an off-shell π^0 which subsequently decays into a pair of photons. We find that the leading contribution is of the latter type. The corresponding operator in the effective low-energy Lagrangian is a consequence the chiral anomaly, and therefore the operator coefficient may be computed exactly from the Wess-Zumino-Witten term [7,8]. The result is

$$\mathcal{O}_{\rm eff}^{(V)} = -\frac{i[2c_u^{(V)} + c_d^{(V)}]e}{16\pi^2 f_\pi \Lambda^2}\epsilon_{\mu\nu\rho\sigma} \times (\bar{\chi}_1\gamma^\mu\chi_2 - \bar{\chi}_2\gamma^\mu\chi_1)F^{\nu\rho}(\partial^\sigma\pi^0), \tag{3.2}$$

where e is the absolute value of the electron charge, f_π is the pion-decay constant, and $F_{\mu\nu}$ is the photon field-strength tensor.

By contrast, for dark-sector particles which couple to the visible sector primarily through the tensor operators in Eq. (2.6), no additional considerations forbid a coupling of the corresponding current operator $\bar{\chi}_i\sigma^{\mu\nu}\chi_j$ to a single photon. Thus, in this case, the leading contribution to the decay width of χ_2 is indeed associated with the processes $\chi_2 \to \chi_1\gamma$. The operator in the effective low-energy Lagrangian which provides the leading contribution to this process can be written in the form

$$\mathcal{O}_{\rm eff}^{(T)} \equiv \frac{i\Lambda_{\rm QCD}}{\Lambda^2}[\xi_u c_u^{(T)} + \xi_d c_d^{(T)}] \times (\bar{\chi}_1\sigma^{\mu\nu}\chi_2 - \bar{\chi}_2\sigma^{\mu\nu}\chi_1)F_{\mu\nu}, \tag{3.3}$$

where $\Lambda_{\rm QCD}$ is the QCD scale and where ξ_u and ξ_d are dimensionless coefficients which parametrize our ignorance of the underlying strong dynamics. Unlike the coefficients in Eq. (3.2), ξ_u and ξ_d are not directly calculable from first principles. Nevertheless, is reasonable to expect that these coefficients are $\mathcal{O}(1)$.

Given the operators in Eqs. (3.2) and (3.3), the corresponding contributions to the χ_2 decay widths are given by

$$\Gamma_{\chi_2\to\chi_1\gamma\gamma\gamma}^{(V)} = \frac{[2c_u^{(V)} + c_d^{(V)}]^2\alpha^3}{25025\cdot 3^4\cdot 2^5\cdot\pi^{10}}\frac{(\Delta m)^{13}}{f_\pi^4 m_\pi^4\Lambda^4},$$
$$\Gamma_{\chi_2\to\chi_1\gamma}^{(T)} = \frac{4\Lambda_{\rm QCD}^2(\Delta m)^3}{\pi\Lambda^4}[\xi_u c_u^{(T)} + \xi_d c_d^{(T)}]^2. \tag{3.4}$$

B. Co-annihilation cross sections

In addition to decays, the operators in Eq. (2.6) also give rise to co-annihilation processes of the form $\chi_1\chi_2 \to \bar{q}q$. Such co-annihilation processes can also be relevant for indirect detection. The corresponding matrix elements can be found, e.g., in Ref. [9]. In both the vector and antisymmetric-tensor cases, we find that the cross section is s-wave even in the $\Delta m \to 0$ limit. Thus, for $\Delta m \ll m_1 \approx m_2$, the thermally averaged cross sections for dark-matter co-annihilation in galactic halos are independent of Δm at leading order and are given by

$$\langle\sigma v\rangle_{\chi_1\chi_2}^{(V)} = \frac{3m_1^2}{\pi\Lambda^4}\sum_q [c_q^{(V)}]^2,$$
$$\langle\sigma v\rangle_{\chi_1\chi_2}^{(T)} = \frac{6m_1^2}{\pi\Lambda^4}\sum_q [c_q^{(T)}]^2. \tag{3.5}$$

Of course, these results reflect the contact-operator coupling between the dark and visible sectors. By contrast, in the regime in which these sectors are coupled by a sufficiently light mediator, dark-matter co-annihilation can

be predominantly p-wave at late times, owing to Sommerfeld enhancement [10].

It is important to note that the expressions in Eq. (3.5) assume that processes of the form $\chi_1\chi_2 \to \bar{q}q$ provide the dominant contribution to the dark-matter co-annihilation cross section and that the effective-theory description of the interactions between the dark and visible sectors in Eq. (2.6) remains valid up to the energy scales $\sqrt{s} \sim m_1 + m_2$ relevant for the co-annihilation of a population of nonrelativistic dark-matter particles. By contrast, if the effective theory breaks down at lower energies, other processes may dominate the co-annihilation cross section. For example, if the contact operators in Eqs. (2.5) and (2.6) arise in the low-energy effective theory due to the presence of a massive vector mediator ϕ of mass m_ϕ in the UV theory, dark-matter co-annihilation to a pair of on-shell ϕ particles typically dominate the thermally averaged cross section when $m_\phi \lesssim m_1 \approx m_2$. Moreover, since the antisymmetric-tensor operator in Eqs. (2.5) and (2.6) does not respect the full electroweak gauge symmetry of the SM, such an operator should be viewed as an effective operator which arises at low energies as a consequence of the electroweak symmetry breaking generated by the nonzero VEV of the SM Higgs field. Thus, one might expect additional annihilation channels involving the Higgs boson to open up for dark-matter masses $m_1 + m_2 \gtrsim m_h \approx 125$ GeV. Such processes can in principle also contribute significantly to the dark-matter co-annihilation rate.

Clearly, the contributions to $\langle\sigma v\rangle^{(V,T)}_{\chi_1\chi_2}$ from additional processes such as those discussed above are highly model-dependent. For sake of generality, we therefore refrain from specifying a particular UV completion for the effective operators in Eqs. (2.5) and (2.6) in this analysis, and instead focus on the regime in which the expressions in Eq. (3.5) provide an accurate description of the thermally averaged co-annihilation cross sections for the vector and antisymmetric-tensor cases.

C. Differential cross sections for inelastic scattering

The matrix element associated with dark-matter scattering is independent of Δm at lowest order. As a result, the main dependence of the differential scattering rate on Δm arises from the phase space.

In general, the differential cross section for a dark-matter particle χ of mass m_χ scattering off a target nucleus of mass m_A can be written in the form

$$\frac{d\sigma^{(V,T)}}{dE_R} = \frac{m_A}{2\mu^2_{\chi A} v^2}\sigma^{(V,T)}_{0A} F^2_{V,T}(E_R), \tag{3.6}$$

where E_R is the recoil energy of scattered nucleus in the detector frame, where v is the detector-frame velocity of χ_i, where $\mu_{\chi A} \equiv m_\chi m_A/(m_\chi + m_A)$ is the reduced mass of the χ-nucleus system, where $F^{(V,T)}(E_R)$ is the appropriate nuclear form factor, and where $\sigma^{(V,T)}_{0A}$ is the scattering cross section at zero momentum transfer. We observe that the vector interaction in Eq. (2.6) contributes to spin-independent (SI) scattering, while the antisymmetric-tensor interaction only contributes to spin-dependent (SD) scattering. Thus, we adopt a parametrization for $\sigma^{(V)}_{0A}$ and $\sigma^{(T)}_{0A}$ of the form

$$\begin{aligned}\sigma^{(V)}_{0A} &= \frac{4\mu^2_{\chi A}}{\pi\Lambda^4}[ZB^{(V)}_p + (A-Z)B^{(V)}_n]^2,\\ \sigma^{(T)}_{0A} &= \frac{16\mu^2_{\chi A}}{\pi\Lambda^4}\frac{J_A+1}{J_A}[\langle S_p\rangle B^{(T)}_p + \langle S_n\rangle B^{(T)}_n]^2.\end{aligned} \tag{3.7}$$

Here Z and A respectively denote the numbers of protons and total nucleons in the target nucleus while J_A is the total nuclear spin and $\langle S_N\rangle$ with $N \in \{p, n\}$ represents the average spin projection of the corresponding nucleon N within the nucleus. The dimensionless couplings $B^{(V,T)}_N$ are given by

$$B^{(V,T)}_N = \sum_q c^{(V,T)}_q \Delta q^{(V,T)}_N \Xi^{(V,T)}_q(m_\chi, \mu_N), \tag{3.8}$$

where the effective nucleon form factors $\Delta q^{(V,T)}_N$ have the values [11]

$$\begin{aligned}\Delta u^{(V)}_p &= \Delta d^{(V)}_n = 2\\ \Delta d^{(V)}_p &= \Delta u^{(V)}_n = 1\\ \Delta s^{(V)}_p &= \Delta s^{(V)}_n = 0\\ \Delta u^{(T)}_p &= \Delta d^{(T)}_n = 0.774\\ \Delta d^{(T)}_p &= \Delta u^{(T)}_n = -0.223\\ \Delta s^{(T)}_p &= \Delta s^{(T)}_n = 0.008.\end{aligned} \tag{3.9}$$

The factor $\Xi^{(V,T)}_q(m_\chi, \mu_N)$ in Eq. (3.8) accounts for the renormalization-group evolution of the effective contact operator from the energy scale m of the dark-matter particle down to the nucleon scale $\mu_N \sim 1$–2 GeV. For the vector case, gauge invariance implies that $\Xi^{(V)}(m_\chi, \mu_N) = 1$. By contrast, for the antisymmetric-tensor case, $\Xi^{(T)}(m_\chi, \mu_N)$ is a product of factors of the form [12]

$$X^{(T)}_q(\mu_i, \mu_j) = \frac{m_q(\mu_j)}{m_q(\mu_i)}\left[\frac{\alpha_s(\mu_j)}{\alpha_s(\mu_i)}\right]^{-16/3\beta_0(\mu_j)}[1 + \mathcal{O}(\alpha_s)], \tag{3.10}$$

where m_q and α_s are the running quark mass and QCD coupling in the $\overline{\text{MS}}$ renormalization scheme, and where $\beta_0(\mu_j) = 11 - (2/3)n_f(\mu_j)$ is the beta function, which depends on the number $n_f(\mu_j)$ of quark flavors q with masses

$m_q > \mu_j$. In particular, for $m_\chi < m_b$ we have $\Xi_q^{(T)}(m_\chi,\mu_N) = X_q^{(T)}(m_\chi,\mu_N)$, while for $m_b < m_\chi < m_t$ we have $\Xi_q^{(T)}(m_\chi,\mu_N) = X_q^{(T)}(m_\chi,m_b)X_q^{(T)}(m_b,m_N)$ and for $m_\chi > m_t$ we have $\Xi_q^{(T)}(m_\chi,\mu_N) = X_q^{(T)}(m_\chi,m_t)X_q^{(T)}(m_t,m_b)X_q^{(T)}(m_b,\mu_N)$.

The differential event rate expected per unit target mass at a given detector can be computed in a straightforward manner from the differential cross section in Eq. (3.6). The result is

$$\frac{dR}{dE_R} = \frac{\rho^{\rm loc}}{m_A m_\chi}\epsilon(E_R)\int_{v>v_{\rm min}} \frac{d\sigma^{(V,T)}}{dE_R} v\mathcal{F}(\vec{v})d^3v, \quad (3.11)$$

where $\rho^{\rm loc}$ is the local energy density of the dark-matter species in question, where $\mathcal{F}(\vec{v})$ is the velocity distribution of that species in the local dark-matter halo, where $\epsilon(E_R)$ is the detector efficiency expressed as a function of E_R, and where $v_{\rm min}$ is the minimum value of $v \equiv |\vec{v}|$ that is kinematically required in order for scattering to take place. This differential rate can also be expressed in the more compact form

$$\frac{dR}{dE_R} = \frac{\rho^{\rm loc}\sigma_0^{(V,T)}}{2m\mu_{\chi A}^2}\epsilon(E_R)F_{V,T}^2(E_R)\mathcal{I}(E_R), \quad (3.12)$$

where we have defined $\mathcal{I}(E_R)$ as a shorthand notation for the dimensionless integral

$$\mathcal{I}(E_R) \equiv \int_{v>v_{\rm min}} \frac{\mathcal{F}(\vec{v})}{v} d^3v. \quad (3.13)$$

In our off-diagonal dark-matter scenario, the scattering processes relevant for direct detection are purely inelastic. Moreover, the event rate generically includes contributions from both the up-scattering of χ_1 particles in the local dark-matter halo and the down-scattering of χ_2 particles. For simplicity, we shall assume that the local energy densities of these two particles are proportional to their respective cosmological number-density fractions $f_1^{(V,T)}(t_{\rm now})$ and $f_2^{(V,T)}(t_{\rm now})$. We take the total local dark-matter energy density to be $\rho_{\rm tot}^{\rm loc} \approx 0.3\ {\rm GeV\,cm^{-3}}$. We shall also take the velocity distributions of both χ_1 and χ_2 to be Maxwellian in the frame of the dark-matter halo, with a one-dimensional velocity dispersion given by $v_0/\sqrt{2}$, where $v_0 \approx 220$ km/s is the local circular velocity. However, this distribution is truncated above the galactic escape velocity $v_{\rm esc} \approx 540$ km/s. For a velocity distribution of this form, the integral over detector-frame velocities in Eq. (3.13) can be performed analytically as a function of $v_{\rm min}$ (see, e.g., Ref. [13]).

The total differential event rate in our off-diagonal dark-matter scenario is simply a sum of the event rates for the up-scattering of χ_1 and the down-scattering of χ_2. Since the coupling coefficients for these two processes are equal—after all, they follow from the same Lagrangian operator—the only difference between the corresponding differential rates is due to kinematics. Indeed, even in the regime in which $\Delta m \ll m_1 \approx m_2$, there yet remains one crucial difference between up-scattering and down-scattering kinematics: a difference in the dependence of the threshold velocity $v_{\rm min}$ on Δm. In general, for a dark-matter particle scattering inelastically with an atomic nucleus, this threshold velocity is given by

$$v_{\rm min} \approx \frac{1}{\sqrt{2m_A E_R}}\left|\frac{E_R m_A}{\mu_{\chi A}} \pm \Delta m\right|, \quad (3.14)$$

where the plus (minus) sign corresponds to the case of a dark-matter particle up- (down-)scattering into a heavier (lighter) dark-sector state.

The total event rate is the sum of the rates for both up-scattering and down-scattering. For compactness, since we are working in the regime in which $\Delta m \ll m_1 \approx m_2$, we shall henceforth replace m_1 and m_2 by a single mass parameter m and retain the dependence on Δm in $v_{\rm min}$. For a detector medium made of different nuclei A of mass fractions w_A, we may express this total rate in the compact form

$$R = \sum_A \frac{\rho_{\rm tot}^{\rm loc} w_A}{2m\mu_{\chi A}^2}\sigma_{0A}^{(V,T)}\left[f_1^{(V,T)}(t_{\rm now})\mathcal{K}_A^+(m) + f_2^{(V,T)}(t_{\rm now})\mathcal{K}_A^-(m)\right] \quad (3.15)$$

by defining

$$\mathcal{K}_A^\pm(m) \equiv \int dE_R F_{V,T}^2(E_R)\epsilon(E_R)\mathcal{I}_\pm(E_R), \quad (3.16)$$

where $\mathcal{I}_\pm(E_R)$ denotes the integral in Eq. (3.13) with the appropriate choice of $v_{\rm min}$ for up-scattering (plus sign) or down-scattering (minus sign).

D. Collider production

The most relevant channels for dark-matter detection at hadron colliders in our off-diagonal dark-matter scenario involve asymmetric pair-production via the process $q\bar{q} \to \chi_1\chi_2$ in association with one or more additional jets, with a photon, or with a $W^\pm$ or Z boson. For the purposes of our eventual study, cross sections for these processes were derived using MadGraph 5 [14] with model input from the FeynRules package [15,16]. Detector-level event rates were obtained using MadGraph 5 for event-generation in conjuction with Pythia 6.4 [17] for fragmentation and hadronization and Delphes 3.3.0 [18] for detector simulation.

IV. CONSTRAINTS

The fundamental parameters which govern the phenomenology of our off-diagonal dark-matter scenario in the

$\Delta m \ll m_1 \approx m_2$ regime are the scale Λ, the mass-splitting parameter Δm, the mass scale m of the dark-matter particles, the operator coefficients $c_u^{(V,T)}$ and $c_d^{(V,T)}$, and the primordial abundance fraction $f_2^{(V,T)}$. Moreover, in the antisymmetric-tensor case, the decay width of χ_2 depends on the unknown $\mathcal{O}(1)$ factors ξ_u and ξ_d appearing in Eq. (3.3).

That said, some of these parameters—for example, ξ_u and ξ_d and the ratio of $c_u^{(V,T)}$ to $c_d^{(V,T)}$—have a less significant impact on the phenomenology than others. Thus, in order to assess the extent to which current data constrain the parameter space of our scenario—and the extent to which future experiments could potentially probe additional regions of that parameter space—we shall adopt two simplifying assumptions with regard to these "secondary" parameters. First, we shall take $c_u^{(V,T)} = c_d^{(V,T)}$. For such a coupling structure, we may absorb these coefficients into the scale Λ without further loss of generality through the redefinition $\Lambda/c_q^{(V,T)} \to \Lambda$. In addition, for concreteness, we shall also assume values for ξ_u and ξ_d such that $M_* \equiv (\xi_u + \xi_d)\Lambda_{\rm QCD} = 1$ GeV. Again, we stress that our results are not particularly sensitive to the precise value of M_*, provided that $M_* \sim \mathcal{O}(\text{GeV})$.

With these assumptions, the number of parameters which govern our scenario reduces to four: Λ, Δm, m, and f_2. Moreover, from amongst these parameters, it is Δm which encapsulates (and in some sense quantifies) the off-diagonal nature of our scenario. Indeed, the $\Delta m \to 0$ limit of our results corresponds to the "diagonal" limit: in this limit we find that τ_2 (the lifetime of the heavier component) becomes infinite (thereby turning off the decay process), up-scattering and down-scattering become identical elastic processes, and so forth. Thus our main interest in this paper lies in studying how the overall phenomenology of our model shifts as we increase Δm from zero.

Before we can proceed, however, we must recognize that a variety of experimental probes of the dark sector already constrain the parameter space of our model. These include indirect-detection probes of both dark-matter decay and co-annihilation in the galactic halo as well as the results of direct-detection experiments and the results of searches for excesses of events in channels with large missing transverse energy at the Large Hadron Collider (LHC). We shall therefore discuss each of these constraints in turn.

A. Decay constraints

When assessing the phenomenological consequences of dark-matter decay in our scenario, the most important consideration is how the lifetime τ_2 of the heavier dark-sector state relates to $t_{\rm now}$ within the region of parameter space in which we are primarily interested—i.e., the region in which $\Delta m \lesssim \mathcal{O}(\text{MeV})$ and $\Lambda \gtrsim \mathcal{O}(\text{GeV})$.

In the vector-interaction case, we see from Eq. (3.4) that $\tau_2 \propto (\Delta m)^{-13}$, which implies that $\tau_2 \gtrsim 10^{14} t_{\rm now}$ within our region of interest. Thus, in this case, we may take

$$f_2^{(V)}(t_{\rm now}) \approx f_2^{(V)}. \tag{4.1}$$

Moreover, since τ_2 is far too long for dark-matter decays to contribute appreciably to event rates at indirect-detection experiments, decay considerations place no meaningful bounds on the parameter space of our off-diagonal dark-matter scenario.

By contrast, in the antisymmetric-tensor-interaction case, we have

$$\tau_2 = \frac{\pi\Lambda^4}{4M_*^2(\Delta m)^3}. \tag{4.2}$$

Thus, in this case, the range of lifetimes accessible within our region of interest extends from the very short to the cosmologically stable—i.e., from $\tau_2 \ll t_{\rm now}$ to $\tau_2 \gg t_{\rm now}$. Thus, the effects of dark-matter decay cannot generally be neglected, and the present-day number-density fraction of χ_2 in our scenario, under the simplifying assumptions discussed above, is given by

$$f_2^{(T)}(t_{\rm now}) = f_2^{(T)} \exp\left[-\frac{4M_*^2(\Delta m)^3 t_{\rm now}}{\pi\Lambda^4}\right]. \tag{4.3}$$

In the antisymmetric-tensor-interaction case, the decays of χ_2 can also give rise to observable signals at indirect-detection experiments. As discussed in Sec. III A, the primary decay channel for χ_2 in the antisymmetric-tensor case is the two-body process $\chi_2 \to \chi_1\gamma$. The resulting primary-photon spectrum from this process consists of a single monochromatic line at $E_\gamma \approx \Delta m \leq \mathcal{O}(\text{MeV})$. Observational limits on such a photon signal can be derived from searches for linelike x-ray signals emanating from sources such as the halo of the Milky Way [19], the Andromeda galaxy [20], dwarf spheroidal galaxies [21,22], and galaxy clusters [23]. Indeed, the results of such searches are used to constrain sterile-neutrino models in which a sterile neutrino of mass m_{ν_s} decays into an active neutrino of mass m_{ν_ℓ} and a photon of energy $E_\gamma \approx E_{\nu_\ell} \approx m_{\nu_s}/2$. In particular, these results place limits on the flux of such photons, a quantity which is proportional to the product of the number density of the sterile neutrino and its decay rate. Adapting these limits to off-diagonal dark-matter scenario is straightforward. Indeed, the only difference is that the bound on the lifetime is suppressed by an additional factor of $2\Delta m/m_2$ because $n_2(t_{\rm now})$ scales inversely with m_2 for fixed abundance.

For a sterile neutrino, one finds that the bound on the corresponding lifetime τ_{ν_s} is essentially independent of m_{ν_s} over a large range of m_{ν_s} and is given by $\tau_{\nu_s} \gtrsim 10^{27}$ s [24].

The corresponding constraint on the parameter space of our off-diagonal dark-matter scenario is therefore

$$f_2^{(T)}(t_{\rm now})\Gamma_2^{(T)} \lesssim \left(\frac{m}{2\Delta m}\right) \times 10^{-27}\ {\rm s}^{-1}. \qquad (4.4)$$

This bound can then be translated into a constraint on the fundamental parameters Λ, Δm, and m which characterize our off-diagonal dark-matter scenario through the use of Eqs. (3.4) and (4.3).

In passing, we also note that if $\Delta m \sim 3.5$ keV, the resulting $E_\gamma \sim 3.5$ keV line from χ_2 decay could potentially explain the excess of x-rays observed in galaxy clusters and in the halos of both Andromeda and the Milky Way (for recent discussions, see, e.g., Refs. [25,26]). In order to determine the region for the number-density fraction f_2 necessary to explain such a signal, we may once again proceed by analogy with the case of a decaying sterile neutrino. For a particle of this sort with an abundance $\Omega_{\nu_s} \sim \Omega_{\rm DM}$, a mass $m_{\nu_s} \sim 7$ keV, and a lifetime in the range $\tau_{\nu_s} \sim (2\text{–}20) \times 10^{27}$ s are required to account for the observed excess. Likewise, in our off-diagonal dark-matter scenario, we can account for such an excess provided that $\Delta m = 3.5$ keV and that

$$f_2^{(T)}(t_{\rm now})\Gamma_2^{(T)} \sim (2\text{–}20) \times \left(\frac{m}{7\ {\rm keV}}\right) \times 10^{27}\ {\rm s}^{-1}. \qquad (4.5)$$

However, we note that recent observations of the Perseus cluster by the Hitomi satelite [27] show no evidence of such a line.

Finally, an additional constraint on dark-matter decays in our scenario arises due to the impact these decays can have on the ionization history of the cosmic microwave background (CMB). Indeed, if a significant population of χ_2 particles decay after recombination, the photons produced by these decays can reionize neutral hydrogen in the intergalactic medium, with observable consequences for the CMB. Planck measurements of the CMB constrain the rate of electromagnetic energy deposited into the CMB at or after the time of recombination $t_{\rm rec} \sim 10^{13}$ s (for reviews, see, e.g., Ref. [28]). For a particle χ with a lifetime $\tau_\chi \gg t_{\rm now}$, the energy deposited in the CMB is roughly equal to the energy $E_{\rm inj}$ injected when it decays. In the case in which this injected energy is transferred entirely to photons or charged particles, Planck data imply a constraint $\Omega_\chi \Gamma_\chi \lesssim 3 \times 10^{-26}\ {\rm s}^{-1}$ on the product of the abundance Ω_χ and the decay width Γ_χ of χ. By contrast, when $\tau_\chi \sim t_{\rm rec}$, the energy deposited in the CMB may be significantly lower in comparison to $E_{\rm inj}$ and the corresponding constraints on Ω_χ and Γ_χ are typically considerably weaker.

In the scenario considered in Ref. [28], essentially all of the initial mass energy m_χ of each decaying χ particle is injected into photons or charged particles at the moment when that particle decays. Thus, $E_{\rm inj} \approx m_\chi$. By contrast, in our off-diagonal dark-matter scenario, the energy injected into such particles through χ_2 decay is $E_{\rm inj} \approx \Delta m$. The corresponding bound on the lifetime of χ_2 in our scenario is therefore

$$\tau_2 \gtrsim \tau_\chi^{\rm max}\left(\frac{\Delta m}{m}\right), \qquad (4.6)$$

where $\tau_\chi^{\rm max}$ is the upper limit on τ_χ taken from Fig. 11 of Ref. [28] for a decaying particle of mass m and mass fraction f_2. Since the band displayed in this figure represents the results of a survey over m_χ and over the decay channels $\chi \to \gamma\gamma$ and $\chi \to e^+e^-$, we extract a value of $\tau_\chi^{\rm max}$ applicable to our scenario in the following way. We note that the bound on τ_χ is weakest in the case in which m_χ—and thus also $E_{\rm inj}$—is small and χ decays into photons rather than e^+e^- pairs. In our off-diagonal dark-matter scenario, each χ_2 likewise decays principally into photons, and the energy $E_{\rm inj}$ injected by each such decay is small. For this reason, we use the value of $\tau_\chi^{\rm max}$ which correspond to the upper edge of this band in deriving our bound on τ_2 for a given mass fraction f_2.

B. Co-annihilation constraints

The leading constraints on the annihilation (or co-annihilation) of dark-matter particles into photons are those derived from Fermi-LAT studies of the gamma-ray spectra Milky-Way dwarf spheroidals [29]. In single-component dark-matter models, this constraint implies an upper bound $\langle\sigma v\rangle_{\bar\chi\chi}^{\rm max}(m_\chi)$ on the thermally averaged annihilation cross section of the dark-matter particle χ, which depends on its mass m_χ.

Since the co-annihilation rates in Eq. (3.5) are approximately independent of Δm in the $\Delta m \ll m_1 \approx m_2$ regime, it is straightforward to translate this bound into a bound on dark-matter co-annihilation in our off-diagonal scenario. Indeed, the only modification we must make is to account for the fact that the initial state involves two different particles with potentially different energy densities $\rho_1(\vec{x})$ and $\rho_2(\vec{x})$. In single-particle dark-matter models, the contribution to the photon flux from any particular point in space is proportional to $\rho_{\rm tot}^2(\vec{x})$, where $\rho_{\rm tot}(\vec{x})$ is the total density of dark matter at that point. By contrast, in our off-diagonal scenario, the corresponding contribution is instead proportional to $\rho_1(\vec{x})\rho_2(\vec{x})$. For simplicity, we shall assume that the halo profiles for χ_1 and χ_2 have the same shape—i.e., that $\rho_1(\vec{x})$ and $\rho_2(\vec{x})$ depend on $\vec{x}$ in the same way and differ only in terms of overall normalization. Moreover, we shall take the normalization factors for $\rho_1(\vec{x})$ and $\rho_2(\vec{x})$ to be proportional to the number-density fractions $f_1^{(T,V)}$ and $f_2^{(T,V)}$. Under these assumptions, the Fermi-LAT constraint on our scenario takes the form

$$\langle\sigma v\rangle^{(V,T)}_{\bar{\chi}_1\chi_2}(m) < \frac{\langle\sigma v\rangle^{\max}_{\bar{\chi}\chi}(m)}{2f_2^{(T,V)}[1-f_2^{(T,V)}]}. \tag{4.7}$$

As discussed in Sec. IV A, the lifetime of χ_2 in the vector case is necessarily significantly longer than the current age of the Universe. In this case, the co-annihilation constraint on the parameter space of our scenario takes the form

$$\frac{12m^2}{\pi\Lambda^4} f_2^{(V)}[1-f_2^{(V)}] < \langle\sigma v\rangle^{\max}_{\bar{\chi}\chi}(m). \tag{4.8}$$

We note that this constraint depends on Λ, m, and $f_2^{(V)}$, but not on the mass splitting Δm. By contrast, in the antisymmetric-tensor case, τ_2 can be of order the age of the Universe. The co-annihilation constraint then takes the form

$$\frac{24m^2}{\pi\Lambda^4} f_2^{(T)}(t_{\rm now})[1-f_2^{(T)}(t_{\rm now})] < \langle\sigma v\rangle^{\max}_{\bar{\chi}\chi}(m). \tag{4.9}$$

In this case, since $f_2^{(T)}(t_{\rm now})$ depends on Δm through Eq. (4.3), the co-annihilation constraint involves all four of our model parameters.

Once again, we emphasize that the constraints in Eqs. (4.8) and (4.9) are derived under the assumption that the contact-operator description of the interaction between the dark and visible sectors in Eqs. (2.5) and (2.6) remains valid up to the energies $\sqrt{s}\sim\mathcal{O}(m)$ relevant for co-annihilation. However, we also note that Fermi-LAT data impose stringent constraints on dark-matter annihilation even in scenarios in which this is not the case—for example, in scenarios involving a light s- and t-channel mediator [30]. Generally speaking, these bounds tend to be roughly similar to the bounds obtained in the contact-operator description. Nevertheless, care should be taken in interpreting the constraints in Eqs. (4.8) and (4.9) within the context of any particular UV theory.

C. Direct-detection constraints

Direct-detection experiments constrain the overall event rate R in Eq. (3.15) for dark-matter scattering off atomic nuclei. In principle, additional information about the scattering kinematics can also be extracted from the recoil-energy spectrum dR/dE_R—information that is sensitive to the kinematic differences between elastic and inelastic scattering. However, the detailed shape of the recoil-energy spectrum is also sensitive to astrophysical properties of the dark-matter distribution in the Milky Way. These include quantities such as the velocity distribution $\mathcal{F}(\vec{v})$, about which there are significant uncertainties. We therefore restrict our attention to bounding the total event rate, deriving an upper limit on R in our off-diagonal dark-matter scenario from the applicable experimental results, and translating this bound into a constraint on the allowed $\{\Lambda,\Delta m,m,f_2^{(V,T)}\}$ parameter space.

As discussed in Sec. IV C, a vector interaction in our off-diagonal dark-matter model contributes to SI scattering, while an antisymmetric-tensor interaction gives rise to SD scattering. We consider each of these cases in turn.

The leading constraints on SI dark-matter scattering are those from the XENON1T, LUX, and PANDA-X experiments. The most stringent limits from XENON1T are based on results obtained for 3.6×10^4 kg days of exposure [31]. These results place an upper bound $R<5\times10^{-5}$ events kg^{-1} day^{-1} on the event rate for events within a recoil-energy range window 3 keV $\le E_R\le$ 50 keV effectively determined by the detector-efficiency function $\epsilon(E_R)$ given in Ref. [31]. The most stringent limits from LUX are based on results obtained with 3.4×10^4 kg days of exposure [32]. For events within the recoil-energy window 1.1 keV $\le E_R\lesssim$ 60 keV, where the upper end of this range is effectively determined by the efficiency function $\epsilon(E_R)$ given in Ref. [32], the corresponding upper bound on the event rate is $R<8\times10^{-5}$ events kg^{-1} day^{-1}. In translating this limit into a constraint on the parameter space of our off-diagonal dark-matter scenario, we assume a Helm form factor [33,34]. Recent results from PANDA-X [35] provide a slight improvement on the XENON1T limits on SI scattering for dark-matter particles of mass $m\gtrsim100$ GeV. However, this slight improvement does not have a significant impact on the region of our parameter space excluded by direct-detection experiments.

In the case of SD scattering, the expected event rate at a given detector depends strongly on the relative strengths of the effective couplings of the dark-sector particles to protons and neutrons. When the coupling to neutrons dominates, the most stringent limits are once again those from the LUX experiment [36], which provides a bound $R<8\times10^{-5}$ events kg^{-1} day^{-1} on the event rate, as discussed above. By contrast, when the coupling to protons dominates, the most stringent limits are those from the PICO-60 experiment [37], which provides a bound $R<1.7\times10^{-3}$ events kg^{-1} day^{-1}. In translating both the LUX and PICO-60 limits into bounds on our parameter space, we make use of the spin fractions and form factors from Ref. [38]. We take the efficiency function for PICO-60 from Ref. [39] and consider only the contribution to the event rate from scattering events with recoil energies $E_R<$ 100 keV at this detector.

In addition to assessing how current direct-detection limits constrain the parameter space of our scenario, we are also interested in determining the extent to which future detectors might further probe that parameter space. In particular, we shall examine the reach provided by two hypothetical future detectors. We model one of these detectors after the proposed LZ experiment [40], which provides increased sensitivity to both SI scattering and SD scattering in which the coupling to neutrons dominates.

We model the other detector after the proposed PICO-500 experiment [41], which provides increased sensitivity to SD scattering in which the coupling to protons dominates. For the former detector, we assume an efficiency function $\epsilon(E_R)$ for the LZ detector which is identical to the efficiency function for LUX, but consider a slightly narrower recoil-energy window $6\ \text{keV} \leq E_R \leq 30\ \text{keV}$, in accord with in Ref. [40]. This gives rise to a conservative estimate $R < 2 \times 10^{-6}\ \text{events}\,\text{kg}^{-1}\,\text{day}^{-1}$ for the limit on the scattering rate. For the latter detector, we assume a sensitivity equivalent to that of PICO-500 [41], which translates into a limit $R < 3 \times 10^{-5}\ \text{events}\,\text{kg}^{-1}\,\text{day}^{-1}$ on the scattering rate, and an efficiency function identical to the efficiency function for PICO-60 [39].

D. Collider constraints

The most relevant channels for dark-matter detection at hadron colliders in our off-diagonal dark-matter scenario involve asymmetric pair-production through the process $q\bar{q} \to \chi_1\chi_2$ in association with one or more additional jets, with a photon, or with a $W^{\pm}$ or Z boson. Since we are assuming here that $\Delta m \lesssim \mathcal{O}(\text{MeV})$, the resulting phenomenology is essentially indistinguishable from that associated with the analogous diagonal production processes in traditional single-component dark-matter models. Constraints on these latter processes are therefore directly applicable to our scenario as well.

The leading constraints on dark-matter production at hadron colliders are those from the analysis by the CMS collaboration [42] at the $\sqrt{s} = 13$ TeV LHC with $35.9\ \text{fb}^{-1}$ of integrated luminosity, which combines results from both the monojet $+ \not{E}_T$ and hadronically decaying $\text{W/Z} + \not{E}_T$ channels. Searches in the monojet $+ \not{E}_T$ [43] and hadronically decaying $\text{W/Z} + \not{E}_T$ [44] channels at the same center-of-mass energy have also been performed by the ATLAS collaboration with $36.1\ \text{fb}^{-1}$ and $3.2\ \text{fb}^{-1}$ of integrated luminosity, respectively. We note that searches for dark-matter production at colliders have been performed in the monophoton $+ \not{E}_T$ [45,46] and leptonically decaying mono-Z $+ \not{E}_T$ [47] channels, as well as channels involving a single Higgs boson in conjunction with substantial $\not{E}_T$ [48–50]. However, the constraints from these searches are generically subleading in comparison with the constraints from the monojet and hadronically decaying mono-W/Z channels. Moreover, we note that since we are considering mass splittings $\Delta m \lesssim \mathcal{O}(\text{MeV})$, additional detection channels which can be relevant for off-diagonal dark-matter scenarios with larger mass splittings—such as those involving a monojet and displaced pions $+ \not{E}_T$ [51] or two energetic photons $+ \not{E}_T$ [52]—do not constrain our parameter-space region of interest.

In assessing the implications of these collider constraints on our off-diagonal dark-matter scenario, it is important to keep in mind that the contact-operator description of the interactions between the dark and visible sectors is valid only at energies comfortably below the scale Λ. At higher energies, we would require a more complete description of the full theory which at low energies gives rise to the effective operators in Eq. (2.5). For this reason, a detailed analysis of the collider bounds on our scenario can only be performed within the context of a particular such theory. For example, the constraints quoted in Ref. [42] are derived for a set of simplified models in which the dark and visible sectors interact via a massive scalar or vector mediator ϕ with a mass m_ϕ.

In this paper, by contrast, we shall seek to maintain generality by refraining from specifying a particular UV completion for the operators in Eq. (2.5). However, for reference, we shall nevertheless derive a heuristic bound on Λ in both the vector and antisymmetric-tensor cases according to the following procedure. For a given choice of m in our scenario, we compute the respective cross sections $\sigma^{(V,T)}(pp \to \chi_1\chi_2 j)$ and $\sigma^{(V,T)}(pp \to \chi_1\chi_2 W/Z)$ for the processes which contribute to the event rate in the monojet $+ \not{E}_T$ and hadronically decaying $\text{W/Z} + \not{E}_T$ channels in our scenario after the imposition of the event-selection criteria outlined in Ref. [42]. In doing this we follow the procedure outlined in Sec. III D. We then compare these cross sections to the corresponding production cross sections $\sigma^{(\phi)}(pp \to \chi\chi j)$ and $\sigma^{(\phi)}(pp \to \chi\chi W/Z)$ obtained for the vector-mediator model considered in Ref. [42] after the imposition of the same cuts. Since $\sigma^{(V,T)}(pp \to \chi\chi j) \propto \Lambda^4$, a lower limit $m_\phi \gtrsim m_{\phi,\text{max}}$ on the mediator mass from the monojet $+ \not{E}_T$ channel corresponds to a bound

$$\Lambda \gtrsim 2 m_{\phi,\text{max}} \left[\frac{\sigma^{(V,T)}(pp \to \chi_1\chi_2 j)}{\sigma^{(\phi)}(pp \to \chi\chi j)} \right]^{1/4} \tag{4.10}$$

on the scale Λ. Note that the factor of two appearing in this expression reflects the difference between our benchmark values for the operator coefficients $c_q^{(V,T)}$ and the benchmark values adopted for couplings in the CMS analysis. A completely analogous bound on Λ can likewise be obtained from the hadronically decaying $\text{W/Z} + \not{E}_T$ channel.

Once again, we emphasize that such bounds on Λ strictly apply only in the regime in which the contact-operator description of the interactions between the dark and visible sectors remains valid up to the energy scales $\sqrt{s} \sim \mathcal{O}(\text{TeV})$ relevant for LHC physics. By contrast, if this assumption does not hold—for example, if the contact interactions in Eq. (2.5) arise due to a light mediator particle which could be produced on shell at the LHC—the collider constraints become highly model-dependent. Indeed, in many cases they become significantly weaker. Moreover, we note that there exists a systematic uncertainty of roughly 40% in our signal-event rates, owing to hadronic physics and soft-QCD

effects. However, we also note that the corresponding uncertainty in our bound on Λ is only around 10%.

Finally, we note that for larger values of Δm than those considered here, a variety of additional collider signatures can arise. For example, in this paper we have focused on the scenario in which the lifetime of χ_2, though potentially shorter than the age of the Universe, is nevertheless long enough that it will not decay within the detection volume of the LHC. For larger values of Δm, however, the decay of the heavier component is more rapid and can thus occur *within* the detection volume. Such scenarios have been considered in the context of colliders [53–59] as well as fixed-target experiments [60,61]. Key features of these scenarios are the detection of Standard-Model particles arising from the decay of the heavier dark particle, potentially with a displaced vertex.

V. RESULTS: A PICTURE OF OFF-DIAGONAL COMPLEMENTARITY

We now turn to examine how the experimental limits discussed in Sec. IV collectively constrain the parameter space of our off-diagonal dark-matter scenario. We present our results as constraint contours in the $(\Lambda, \Delta m)$ plane for a set of benchmark values $m = \{10\ \text{GeV}, 100\ \text{GeV}, 1\ \text{TeV}\}$ for the dark-matter mass scale. A set of different contours corresponding to different choices $f_2^{(V,T)} = \{0, 0.5, 1\}$ for the primordial abundance fraction is included for the decay, co-annihilaion, and direct-detection constraints, which are sensitive to the value of $f_2^{(T,V)}$. The results for the case of a vector interaction are shown in Fig. 1, while the results for the case of an antisymmetric-tensor interaction are shown in Fig. 2.

The yellow shaded regions correspond to the exclusion regions associated with the Fermi-LAT PASS8 co-annihilation bounds for $f_2^{(V,T)} = 0.5$ (light yellow) and $f_2^{(V,T)} = 1$ (dark yellow). The orange shaded regions correspond to the exclusion regions from reionization effects on the CMB for $f_2^{(V,T)} = 0.5$ (dark orange) and $f_2^{(V,T)} = 1$ (light orange). The gray shaded regions correspond to the exclusion contours from x-ray line searches for $f_2^{(V,T)} = 0.5$ (dark gray) and $f_2^{(V,T)} = 1$ (light gray). Constraint contours corresponding to bounds from individual direct-detection experiments are shown for $f_2^{(V,T)} = 0$ (solid lines), $f_2^{(V,T)} = 0.5$ (dotted lines), and $f_2^{(V,T)} = 1$ (dashed lines). Projected limits for future direct-detection experiments are displayed in the same way. The purple shaded region corresponds to the region which is excluded by the most conservative case, wherein $f_2^{(V,T)} = 0$ and the signal contribution is due to up-scattering alone. The green line appearing in the $m = 10$ GeV and $m = 100$ GeV panels of Figs. 1 and 2 corresponds to the combined upper limit derived from monojet $+ \not{E}_T$ and hadronically decaying $\mathrm{W/Z} + \not{E}_T$ searches at CMS for the case of a contact interaction. This line is omitted in the $m = 1$ TeV panels, since the contact-operator description is not valid within the region of parameter space constrained by these searches for such a large value of m.

The striped gray region at the top of each panel of Figs. 1 and 2 indicates the region of parameter space within which decay channels for χ_2 involving $e + e^-$ pairs in the final state are kinematically accessible. We emphasize that while this region lies outside our regime of interest, it is not necessarily excluded in its entirety. Finally, the green stars in Fig. 2 indicate the points in parameter space at which our scenario is capable of explaining the 3.5-keV x-ray line.

As discussed near the beginning of Sec. IV, the parameter Δm captures (and in some sense quantifies) the off-diagonality inherent in our dark-matter scenario. Indeed, as $\Delta m \to 0$, we recover the bounds and constraints that would be expected for a "diagonal," single-component dark-matter scenario. Our main interest, therefore, is in determining how the behavior of these constraints evolves—and what new constraints may appear—as Δm increases from zero within each of the panels in Figs. 1 and 2.

A. Vector interaction

The constraint contours for the case of a vector interaction are shown in Fig. 1. Since χ_2 is extremely stable in this case, as discussed in Sec. IV A, experimental limits from dark-matter decay—including both those from x-ray instruments and those from reionization effects on the CMB—yield no meaningful bounds on our parameter space.

The longevity of χ_2 in the vector case also has an important impact on co-annihilation constraints. Co-annihilation requires that a non-negligible population of both χ_1 and χ_2 be present in the dark-matter halo of the astrophysical object under observation. Indeed, Eq. (4.7) implies that the co-annihilation constraint on the parameter space of our scenario is the most severe when equal numbers of χ_1 and χ_2 are present in the halo and disappears altogether when only one species is present. Since χ_2 is stable on cosmological timescales in the vector case, we have $f_2^{(T,V)}(t_{\text{now}}) \approx f_2^{(T,V)}$. As a result, the co-annihilation constraint contours for both $f_2^{(T,V)} = 0$ and $f_2^{(T,V)} = 1$ vanish. Moreover, since the constraint is essentially independent of Δm in this case, the constraint contour for $f_2^{(T,V)} = 0.5$ appearing in each panel of Fig. 1 is effectively a vertical line.

For small Δm, we find that direct-detection constraints generically provide the strongest bounds on Λ. However, we see that direct-detection experiments quickly lose sensitivity once Δm exceeds a certain threshold. This behavior is the result of a nontrivial interplay between scattering kinematics and detector-performance considerations. For up-scattering, the additional energy Δm required to produce the final-state χ_2 particle must be supplied by the kinetic energy of the

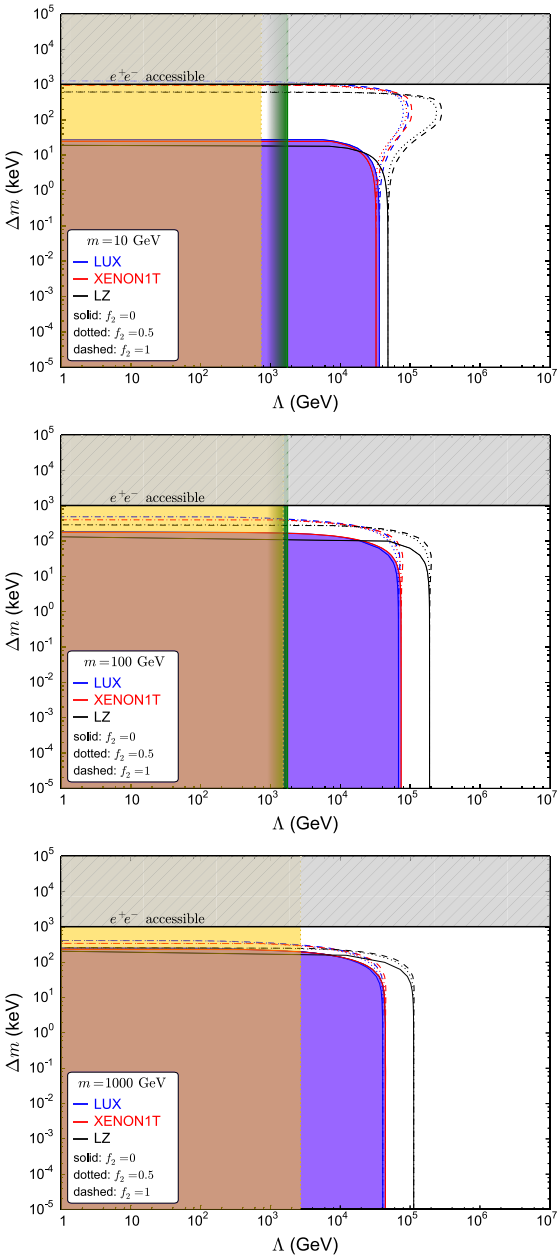

FIG. 1. Constraints on the parameter space of our scenario for the case of the vector interaction in Eq. (2.6). The upper, middle, and lower panels correspond respectively to the choices $m = \{10, 100, 1000\}$ GeV. The yellow shaded region is excluded by co-annihilation limits from Fermi-LAT for $f_2^{(V)} = 0.5$. The magenta shaded region is excluded by combined direct-detection limits from LUX and XENON1T for the conservative case of $f_2^{(V)} = 0$. Individual constraint contours from both LUX and XENON1T, as well as contours representing the projected reach of LZ, are shown for $f_2^{(V)} = 0$ (solid curves), $f_2^{(V)} = 0.5$ (dotted curves), and $f_2^{(V)} = 1$ (dashed curves). The green line represents the naïve bound from CMS searches in contact-operator approximation. For further details, see text.

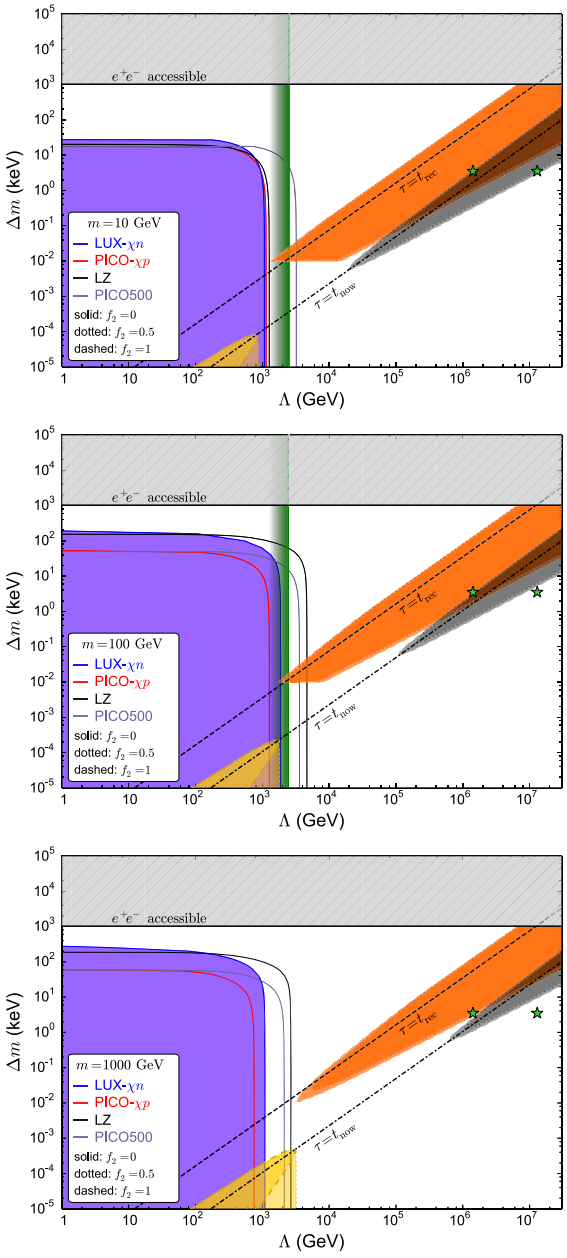

FIG. 2. Constraints on the parameter space of our scenario for the case of the antisymmetric-tensor interaction in Eq. (2.6). The upper, middle, and lower panels correspond respectively to the choices $m = \{10, 100, 1000\}$ GeV. The yellow shaded regions are excluded by co-annihilation limits from Fermi-LAT, while the orange shaded regions are excluded by reionization limits and the gray shaded regions are excluded by x-ray searches. The magenta shaded region is excluded by combined direct-detection limits from LUX and PICO-60. Individual constraint contours from both LUX and PICO-60, as well as contours representing the projected reach of both LZ and PICO-500, are also shown. Note that the direct-detection curves for all benchmark choices of $f_2^{(T)}$ effectively coincide. The green line represents the naïve bound from CMS searches in contact-operator approximation. The green stars indicate the points in parameter space consistent with the purported 3.5 keV line observed in galactic clusters and in the Milky Way and Andromeda halos. For further details, see text.

incoming χ_1 particle. Since the velocity distribution $\mathcal{F}(\vec{v})$ for dark-matter in the Milky-Way halo is suppressed at large v—and indeed drops to zero for $v \geq v_{\rm esc}$—this energy threshold becomes prohibitively large for sufficiently large Δm. By contrast, for down-scattering, the scattering process is exothermic, with the additional mass energy Δm released by the incoming χ_2 providing an additional contribution to the kinetic energies of the final-state particles. For this reason, we find that the presence of even a tiny present-day number-density fraction $f_2^{(V)}(t_{\rm now}) \approx f_2^{(V)}$ for the heavier dark-matter species results in a dramatic increase in sensitivity in the region above the Δm threshold for up-scattering relative to the sensitivity obtained for $f_2^{(V)}(t_{\rm now}) = 0$.

Indeed, it is apparent from Fig. 1 that direct-detection constraints are typically strongest when down-scattering dominates and $\Delta m \sim \mathcal{O}(1\text{–}100\ {\rm keV})$, as is apparent in the constraint contours obtained for $f_2^{(T,V)} = 1$. However, for sufficiently large Δm, typical E_R values associated with down-scattering events lie above the recoil-energy window associated with these experiments—a window whose upper limit is effectively determined by efficiency considerations and event-selection requirements. Thus, for down-scattering as well as up-scattering, there exists an upper limit on the value of Δm to which direct-detection experiments are sensitive.

As discussed in Sec. IV D, collider constraints on our scenario are essentially independent of Δm for $\Delta m \ll m$. Consequently, the corresponding constraint contours in the panels of Fig. 1 also appear as vertical lines. For $m = 10$ GeV, the constraints are roughly comparable to those from co-annihilation. However, as m increases, the collider constraints become weaker while the co-annihilation constraints become stronger. The decrease in collider sensitivity is to be expected, given that the pair-production rate at colliders decreases with increasing m when m is large. On the other hand, the increase in indirect-detection sensitivity to co-annihilation is due primarily to an increase in the energy of the visible particles produced by co-annihilation. We note that while the number densities of our dark-matter species decrease with increasing m, this suppression is compensated by an increase in the co-annihilation cross section.

In summary, for the case of a vector interaction, direct-detection constraints provide the most stringent bounds on—and the best projected reach within—the parameter space of our scenario. For $\Delta m \lesssim 100$ keV, current limits from LUX and XENON1T exclude values of Λ up to 10–100 TeV. However, we also see that for larger mass splittings in the range $100\ {\rm keV} \lesssim \Delta m \lesssim 1$ MeV, indirect-detection bounds from co-annihilation play an important role, filling in the "gap" between where direct-detection experiments lose sensitivity—especially when $f_2^{(V)}$ is small—and where dark-matter decay channels to final states involving e^+e^- pairs open up.

B. Tensor interaction

The constraint contours for the case of a tensor interaction are shown in Fig. 2. We observe that in this case far shorter lifetimes for χ_2 can be realized within our parameter-space region of interest than in the case of a vector interaction. The behavior of τ_2 within the $(\Lambda, \Delta m)$ plane can be inferred from Eq. (4.2), which indicates that $\tau_2 \propto \Lambda^4/(\Delta m)^3$. Thus, we see that lifetime of χ_2 increases as one moves downward and to the right in each panel of Fig. 2, and that contours of constant τ_2 are straight lines running from the lower left to the upper right. For reference, we explicitly include two such contours (the thick dashed lines) on each panel of this figure. The first corresponds to a lifetime $\tau_2 = t_{\rm now}$, which is the time scale relevant for x-ray line searches. The second corresponds to a lifetime $\tau_2 = t_{\rm rec}$, which is the timescale relevant for CMB physics.

We see that the region of our parameter space most strongly constrained by x-ray line searches in each panel of Fig. 2 is that in which $\tau_2 \sim t_{\rm now}$. The corresponding constraint contours, which are given by Eq. (4.4), depend on the fundamental scales Λ, Δm, and m which characterize our scenario through τ_2 and through the ratio $\Delta m/m$, which represents the fraction of the mass energy of χ_2 which is transferred to the kinetic energies of the decay products. Indeed, within each panel—i.e., for fixed m—we see that the x-ray constraints grow weaker as Δm decreases. Likewise, comparing the different panels of the figure, we also see that these constraints grow weaker as m increases. Moreover, we also see that the x-ray constraints become weaker as $f_2^{(T)}$, which specifies the number density of χ_2 in the early Universe, decreases.

By contrast, we see that the region of parameter space most strongly constrained by reionization limits in each panel of Fig. 2 is that in which τ_2 is near or slightly above $t_{\rm rec}$. For $\tau_2 \lesssim t_{\rm rec}$, the majority of χ_2 particles decay well before recombination; thus, the energy injected by those decays does not contribute to reionization effects on the CMB. By contrast, for $\tau_2 \gtrsim t_{\rm rec}$, the majority of χ_2 particles decay after recombination and stringent constraints on our parameter space arise. Indeed, for lifetimes in the range $t_{\rm rec} \lesssim \tau_2 \lesssim t_{\rm now}$, these constraints are competitive with the x-ray constraints discussed above, whereas for $\tau_2 \gg t_{\rm now}$, those x-ray constraints dominate. Once again, we observe that the overall shape of the constraint contours from reionization is essentially determined by the interplay between τ_2 and the ratio $\Delta m/m$. As a result, this shape is similar to the overall shape of the x-ray contours. The only salient difference is that the reionization contours are cut off below $\Delta m \sim 13.6$ eV, since a photon with E_γ below this threshold cannot ionize neutral hydrogen.

We observe that the region of our parameter space in Fig. 2 excluded by Fermi-LAT limits on dark-matter co-annihilation differs significantly from the region excluded in Fig. 1. This is ultimately due to the fact that

co-annihilation requires a significant population of χ_2 to be present in the halos of such galaxies at present time. Thus, just as with the x-ray constraints discussed above, we find that co-annihilation limits place no meaningful bounds on our parameter space when $\tau_2 \ll t_{\rm now}$. However, for $\tau_2 \gtrsim t_{\rm now}$, an observable co-annihilation signal may indeed arise. In situations in which a substantial primordial abundance is generated for both χ_1 and χ_2—as is the case, for example, for our number-density fraction benchmark $f_2^{(T)} = 0.5$—the co-annihilation bound on Λ from Eq. (4.9) is not particularly sensitive to the value of Δm.

By contrast, in situations in which the primordial abundance of χ_1 is negligible and essentially all of the dark matter is initially in the χ_2 state—as is the case for our number-density fraction benchmark $f_2^{(T)} = 1$—a substantial co-annihilation rate can only be achieved if a non-negligible population of χ_1 particles is subsequently generated by χ_2 decays on cosmological time scales. On the one hand, this means that if $\tau_2 \gg t_{\rm now}$, essentially all of the dark matter will still be in the χ_2 state at present time, and the co-annihilation rate will be negligible. On the other hand, if $\tau_2 \ll t_{\rm now}$, essentially all of the dark matter will be in the χ_1 state at present time, as discussed above, and the co-annihilation rate will likewise be negligible. Indeed, for $f_2^{(T)} \approx 1$, a lifetime $\tau_2 \sim t_{\rm now}$ is required in order to achieve a non-negligible co-annihilation signal. In this case, the corresponding constraint contours exhibit a clear sensitivity to the value of Δm, as evident in Fig. 2.

As discussed in Sec. III C, the primary difference between the direct-detection phenomenology which stems from a vector interaction and that which stems from an antisymmetric-tensor interaction is that the former gives rise to SI scattering, whereas the latter only gives rise to SD scattering. Since the limits on SI scattering are considerably more stringent than those on SD scattering, the direct-detection constraints on Λ in Fig. 2 are significantly weaker than those in Fig. 1. However, another important difference arises due to a difference between the characteristic ranges τ_2 associated with the vector and tensor interactions in our off-diagonal dark-matter scenario. Throughout almost all of the parameter space in Fig. 2 within which direct-detection experiments are sensitive to inelastic scattering in our scenario, we have $\tau_2 \ll t_{\rm now}$. This implies that essentially all of the dark-matter in the Milky-Way halo at present time is in the χ_1 state. The only non-negligible contribution to the event rate at direct-detection experiments is therefore due to up-scattering, which is kinematically suppressed, as discussed above—especially for large Δm. The only region of parameter space in which χ_2 is cosmologically stable and in which one might expect a direct-detection signal is a region in which Δm is so small that there is essentially no kinematic difference between up-scattering and down-scattering. Thus, the direct-detection phenomenology that arises in the case of an antisymmetric-tensor interaction is essentially independent of $f_2^{(T)}$, and the constraint contours for all three of our benchmark choices for this parameter coincide.

The collider constraints on our parameter space in the antisymmetric-tensor case are independent of Δm, as they were in the vector case. Thus, the corresponding constraint contours in the panels of Fig. 2 likewise appear as vertical lines. However, we see that in the case of an antisymmetric-tensor interaction, collider constraints and the direct-detection constraints are quite competitive. Indeed, we see that for $\Delta m \lesssim 10$ keV, the combined monojet and hadronically decaying W/Z bounds from ATLAS currently represent the leading constraint on Λ. However, we also see that the projected reach of the LZ experiment will supersede this. Perhaps even more importantly, however, colliders represent essentially the only probe of the region of parameter space in which $10\ {\rm keV} \lesssim \Delta m \lesssim 1$ MeV and $\Lambda \lesssim 1$ TeV.

In summary, in the case of a tensor interaction, a picture of dark-matter complementarity emerges in which experimental probes of the dark sector mostly cover different, nonoverlapping regions of our parameter space. For $\Delta m \lesssim 100$ keV and $\Lambda \lesssim 1$ TeV, direct-detection experiments provide excellent coverage of this parameter space, and results from LZ and PICO-500 are projected to extend that coverage over significantly higher values of Λ in the near future. For larger values of Λ, indirect detection plays the dominant role in probing our parameter space. Gamma-ray detectors sensitive to dark-matter co-annihilation provide some coverage for smaller Λ and Δm, while probes of dark-matter decay, including both x-ray line searches and observations of the CMB, provide coverage for larger values of these paramaters.

One salient difference between the complementarity picture which emerges in the antisymmetric-tensor case, in comparison with the one which emerges in the vector case, is that there exists a range of mass splittings $100\ {\rm keV} \lesssim \Delta m \lesssim 1$ MeV for which the only bounds on Λ are those from colliders. However, as discussed in Sec. IV D, these bounds are highly model-dependent. These considerations motivate efforts to explore this region of parameter space using other, complementary probes of the dark sector as well. One promising possibility is that by extending the range of nuclear-recoil energies accessible at direct-detection experiments to higher E_R, future such experiments could provide more robust coverage of some or even all of this region.

VI. CONCLUSIONS AND OUTLOOK

Recent years have seen increasing focus on multi-component dark sectors. Indeed, a particularly dramatic example of this is the so-called Dynamical Dark Matter framework of Refs. [62–64]. However, such multi-component dark sectors give rise to two general classes

of dark-matter processes: "diagonal" processes that involve only dark-matter species, and "off-diagonal" processes that involve two (or more) dark-matter species. Normally, one might expect the experimental signals from diagonal processes to dominate those from off-diagonal processes. However, as we have seen, there exist particular multi-component dark-matter scenarios in which the diagonal processes are absent or suppressed, and in which it is the *off*-diagonal processes which dominate the resulting phenomenology.

In this paper, we have examined the phenomenology of such off-diagonal dark-matter scenarios—scenarios in which the dark sector couples to the visible sector primarily through interactions involving two different dark-sector fields. Scenarios of this sort give rise to inelastic scattering at direct-detection experiments, dark-matter co-annihilation in the halos of galaxies, asymmetric pair-production processes at colliders, and dark-matter decay. We have shown that such off-diagonal dark-matter scenarios naturally arise when the dark sector consists of a Dirac fermion χ which is subsequently split into a pair of nearly degenerate mass eigenstates χ_1 and χ_2 by a small Majorana mass. In such "pseudo-Dirac" models, if χ couples to the visible sector primarily through operators involving the vector bilinear $\bar{\chi}\gamma^\mu\chi$ or the tensor bilinear $\bar{\chi}\sigma^{\mu\nu}\chi$, the resulting couplings between these mass eigenstates and the visible sector are purely off-diagonal. We have examined the phenomenology which follows from such scenarios both in the case of a vector interaction and in the case of an antisymmetric-tensor interaction, and we have examined the picture of dark-matter complementarity which arises in each case.

A few comments are in order. First, we emphasize that for sake of generality we have refrained from specifying a UV completion for either of the contact operators appearing in Eq. (2.6). For this reason, the collider constraints we have taken into account in constraining our off-diagonal dark-matter scenario are solely those associated with model-independent dark-matter detection channels such as monojet $+ \not{E}_T$, monophoton $+ \not{E}_T$, etc., which pertain to the contact-operator description. In the regime in which $\Lambda \lesssim \mathcal{O}(\mathrm{TeV})$, the contact-operator formulation is no longer reliable and other channels may play an important role in the collider phenomenology of the scenario. For example, if the relevant contact operator in Eq. (2.6) results from integrating out a light mediator, processes in which the mediator is produced on shell may provide stronger constraints than the model-independent interactions listed above. For this reason, we emphasize that the collider bounds presented in Figs. 1 and 2 should be interpreted only heuristically and are only strictly valid when $\Lambda \gg \mathcal{O}(\mathrm{TeV})$. Similar caveats pertain to the co-annihilation constraints on our scenario, which are only strictly valid when $\Lambda \gg \mathcal{O}(m)$.

Second, we note that while the recoil-energy thresholds for the direct-detection experiments relevant for this analysis are currently $\mathcal{O}(\mathrm{keV})$, future experiments could potentially achieve a comparable sensitivity with $\mathcal{O}(\mathrm{eV})$ thresholds. Such experiments would potentially be able to discriminate between up-scattering, down-scattering, and elastic scattering on the basis of the recoil-energy spectrum for mass splittings down to $\Delta m \sim \mathcal{O}(\mathrm{eV})$. For such small values of Δm, the lifetime of χ_2 can be comparable to the age of the Universe in the case of an antisymmetric-tensor interaction, implying that down-scattering might also be distinguishable at direct-detection experiments in this case.

Finally, in this analysis, we have only considered tree-level interactions between the dark and visible sectors of the form specified in Eq. (2.6). However, we note that these tree-level operators also generically give rise to additional interactions at the loop level. For example, operators arise at one loop which contribute to elastic scattering at direct-detection experiments. While such process are expected to be suppressed, they can nevertheless be important in regions of parameter space within which other probes of the dark sector are insensitive.

ACKNOWLEDGMENTS

We are happy to thank Danny Marfatia and Farinaldo Queiroz for discussions. We also thank CETUP* (the Center for Theoretical Underground Physics and Related Areas) for hospitality during its 2015 Summer Program, where this work was initiated. The research activities of K. R. D. and D. Y. are supported in part by the Department of Energy under Grant No. DE-FG02-13ER41976 (DE-SC0009913), while those of J. K. are supported in part by NSF CAREER Grant No. PHY-1250573 and those of B. T. are supported in part by NSF Grant No. PHY-1720430. The research activities of K. R. D. are also supported in part by the National Science Foundation through its employee IR/D program. The opinions and conclusions expressed herein are those of the authors and do not represent any funding agencies.

[1] For reviews, see, e.g. G. Jungman, M. Kamionkowski, and K. Griest, Phys. Rep. **267**, 195 (1996); J. D. Lewin and P. F. Smith, Astropart. Phys. **6**, 87 (1996); D. Hooper, arXiv:0901.4090; N. Weiner, in *Proceedings of TASI 2009*, http://physicslearning2.colorado.edu/tasi/tasi_2009/tasi_2009.htm; J. L. Feng, Annu. Rev. Astron. Astrophys. **48**, 495 (2010); R. W. Schnee, arXiv:1101.5205; M. Lisanti, arXiv:1603.03797.

[2] S. Arrenberg *et al.*, arXiv:1310.8621.

[3] K. R. Dienes, J. Kumar, B. Thomas, and D. Yaylali, Phys. Rev. Lett. **114**, 051301 (2015).

[4] D. Tucker-Smith and N. Weiner, Phys. Rev. D **64**, 043502 (2001).

[5] J. Kopp, T. Schwetz, and J. Zupan, J. Cosmol. Astropart. Phys. 02 (2010) 014.

[6] P. A. R. Ade *et al.* (Planck Collaboration), Astron. Astrophys. **594**, A13 (2016).

[7] J. Wess and B. Zumino, Phys. Lett. **37B**, 95 (1971).

[8] E. Witten, Nucl. Phys. **B223**, 422 (1983).

[9] J. Kumar and D. Marfatia, Phys. Rev. D **88**, 014035 (2013).

[10] A. Das and B. Dasgupta, Phys. Rev. Lett. **118**, 251101 (2017).

[11] T. Bhattacharya, V. Cirigliano, S. D. Cohen, R. Gupta, A. Joseph, H.-W. Lin, and B. Yoon (PNDME Collaboration), Phys. Rev. D **92**, 094511 (2015).

[12] R. J. Hill and M. P. Solon, Phys. Rev. D **91**, 043505 (2015).

[13] C. Savage, G. Gelmini, P. Gondolo, and K. Freese, J. Cosmol. Astropart. Phys. 04 (2009) 010.

[14] J. Alwall, M. Herquet, F. Maltoni, O. Mattelaer, and T. Stelzer, J. High Energy Phys. 06 (2011) 128.

[15] N. D. Christensen and C. Duhr, Comput. Phys. Commun. **180**, 1614 (2009).

[16] A. Alloul, N. D. Christensen, C. Degrande, C. Duhr, and B. Fuks, Comput. Phys. Commun. **185**, 2250 (2014).

[17] T. Sjostrand, S. Mrenna, and P. Z. Skands, J. High Energy Phys. 05 (2006) 026.

[18] S. Ovyn, X. Rouby, and V. Lemaitre, arXiv:0903.2225.

[19] A. Boyarsky, J. Nevalainen, and O. Ruchayskiy, Astron. Astrophys. **471**, 51 (2007).

[20] A. Boyarsky, D. Iakubovskyi, O. Ruchayskiy, and V. Savchenko, Mon. Not. R. Astron. Soc. **387**, 1361 (2008).

[21] D. Malyshev, A. Neronov, and D. Eckert, Phys. Rev. D **90**, 103506 (2014).

[22] O. Ruchayskiy *et al.*, Mon. Not. R. Astron. Soc. **460**, 1390 (2016).

[23] A. Boyarsky, O. Ruchayskiy, and M. Markevitch, Astrophys. J. **673**, 752 (2008).

[24] A. Boyarsky and O. Ruchayskiy, arXiv:0811.2385.

[25] F. S. Queiroz, arXiv:1605.08788.

[26] M. Drewes *et al.*, J. Cosmol. Astropart. Phys. 01 (2017) 025.

[27] F. A. Aharonian *et al.* (Hitomi Collaboration), Astrophys. J. **837**, L15 (2017).

[28] T. R. Slatyer and C. L. Wu, Phys. Rev. D **95**, 023010 (2017).

[29] M. Ackermann *et al.* (Fermi-LAT Collaboration), Phys. Rev. Lett. **115**, 231301 (2015).

[30] L. M. Carpenter, R. Colburn, J. Goodman, and T. Linden, Phys. Rev. D **94**, 055027 (2016).

[31] E. Aprile *et al.* (XENON Collaboration), Phys. Rev. Lett. **119**, 181301 (2017).

[32] D. S. Akerib *et al.* (LUX Collaboration), Phys. Rev. Lett. **118**, 021303 (2017).

[33] R. H. Helm, Phys. Rev. **104**, 1466 (1956).

[34] J. Engel, Phys. Lett. B **264**, 114 (1991).

[35] X. Cui *et al.* (PandaX-II Collaboration), Phys. Rev. Lett. **119**, 181302 (2017).

[36] D. S. Akerib *et al.* (LUX Collaboration), Phys. Rev. Lett. **118**, 251302 (2017).

[37] C. Amole *et al.* (PICO Collaboration), Phys. Rev. Lett. **118**, 251301 (2017).

[38] P. Klos, J. Menndez, D. Gazit, and A. Schwenk, Phys. Rev. D **88**, 083516 (2013); **89**, 029901(E) (2014).

[39] C. Amole *et al.* (PICO Collaboration), Phys. Rev. D **93**, 052014 (2016).

[40] B. J. Mount *et al.*, arXiv:1703.09144.

[41] S. Fallows, talk given at TAUPP 2017, https://indico.cern.ch/event/606690/contributions/2623446/.

[42] CMS Collaboration, Report No. CMS-PAS-EXO-16-048.

[43] ATLAS collaboration, Report No. ATLAS-CONF-2017-060.

[44] M. Aaboud *et al.* (TLAS Collaboration), Phys. Lett. B **763**, 251 (2016).

[45] M. Aaboud *et al.* (ATLAS Collaboration), Eur. Phys. J. C **77**, 393 (2017).

[46] A. M. Sirunyan *et al.* (CMS Collaboration), J. High Energy Phys. 10 (2017) 073.

[47] A. M. Sirunyan *et al.* (CMS Collaboration), J. High Energy Phys. 03 (2017) 061.

[48] M. Aaboud *et al.* (ATLAS Collaboration), Phys. Lett. B **765**, 11 (2017).

[49] A. M. Sirunyan *et al.* (CMS Collaboration), arXiv:1703.05236.

[50] M. Aaboud *et al.* (ATLAS Collaboration), arXiv:1706.03948.

[51] Y. Bai and T. M. P. Tait, Phys. Lett. B **710**, 335 (2012).

[52] R. Primulando, E. Salvioni, and Y. Tsai, J. High Energy Phys. 07 (2015) 031.

[53] Y. Bai and T. M. P. Tait, Phys. Lett. B **710**, 335 (2012).

[54] N. Weiner and I. Yavin, Phys. Rev. D **86**, 075021 (2012).

[55] E. Izaguirre, G. Krnjaic, and B. Shuve, Phys. Rev. D **93**, 063523 (2016).

[56] M. J. Baker *et al.*, J. High Energy Phys. 12 (2015) 120.

[57] M. Buschmann, S. El Hedri, A. Kaminska, J. Liu, M. de Vries, X. P. Wang, F. Yu, and J. Zurita, J. High Energy Phys. 09 (2016) 033.

[58] S. El Hedri, A. Kaminska, M. de Vries, and J. Zurita, J. High Energy Phys. 04 (2017) 118.

[59] O. Buchmueller, A. De Roeck, K. Hahn, M. McCullough, P. Schwaller, K. Sung, and T. T. Yu, J. High Energy Phys. 09 (2017) 076.

[60] D. E. Morrissey and A. P. Spray, J. High Energy Phys. 06 (2014) 083.

[61] E. Izaguirre, Y. Kahn, G. Krnjaic, and M. Moschella, Phys. Rev. D **96**, 055007 (2017).

[62] K. R. Dienes and B. Thomas, Phys. Rev. D **85**, 083523 (2012).

[63] K. R. Dienes and B. Thomas, Phys. Rev. D **85**, 083524 (2012).

[64] K. R. Dienes and B. Thomas, Phys. Rev. D **86**, 055013 (2012).